Ab Initio Molecular Dynamics Investigation of Molten Fe–Si–O in Earth's Core

Dongyang Huang[1] (iD), James Badro[1,2] (iD), John Brodholt[3] (iD), and Yunguo Li[3] (iD)

[1]Institut de Physique du Globe de Paris, Sorbonne Paris Cité, 75005, Paris, France, [2]École Polytechnique Fédérale de Lausanne, Lausanne, Switzerland, [3]Department of Earth Sciences, University College London, London, UK

Abstract Silicon and oxygen are potential light elements in Earth's core because their stronger affinity to metal observed with increasing temperature posits that significant amounts of both can be incorporated into the core. It was proposed that an Fe–Si–O liquid alloy could expel SiO_2 at the core-mantle boundary during secular cooling, leaving the core with either silicon or oxygen, not both. This was recently challenged in a study showing no exsolution but immiscibility in the Fe–Si–O system. Here we investigate the liquidus field of Fe–Si and Fe–O binaries and Fe–Si–O ternaries at core-mantle boundary pressures and temperatures using ab initio molecular dynamics. We find that the liquids remain well mixed with ternary properties identical to mixing of binary properties. Two-phase simulations of solid SiO_2 and liquid Fe show dissolution at temperatures above 4100 K, suggesting that SiO_2 crystallization as well as liquid immiscibility in Fe–Si–O is unlikely to occur in Earth's core.

Plain Language Summary The standard hypothesis is that Earth's core inherited its composition (iron-nickel alloy + lighter elements such as Si, O, S, and C) during core formation by interaction with Earth's silicate magma ocean and has since remained fixed and well mixed through geological time. It was recently proposed, on the basis of high-pressure experiments, that silicon and oxygen dissolved in the core could crystallize as SiO_2 at the core-mantle boundary during secular cooling, challenging our understanding of core composition and evolution. While other experimental studies have not corroborated these findings, a recent study involving experiments and calculations proposed no SiO_2 exsolution but rather liquid-liquid immiscibility in the iron-silicon-oxygen system. In this study, we use ab initio molecular dynamics simulations to theoretically investigate the liquidus field of Fe–Si, Fe–O and Fe–Si–O alloys. We find that (1) the liquid alloys remain stable and well mixed, with the volumes of iron, silicon, and oxygen mixing ideally at core conditions; (2) no sign of SiO_2 crystallization or phase separation (i.e., immiscibility); and (3) simulations of solid SiO_2 in contact with liquid Fe show mixing of both phases, ruling out silica precipitation out of the core.

1. Introduction

The Earth's core was formed by gravitational segregation of liquid iron and molten silicates in a magma ocean during primordial differentiation (Ringwood, 1959). While siderophile elements are stripped by iron that now forms the metallic core, some nominally lithophile elements are also found to dissolve in iron, namely, Si and O (e.g., Asahara et al., 2007; Badro et al., 2018; Blanchard et al., 2017; Bouhifd & Jephcoat, 2011; Chabot & Agee, 2003; Fischer et al., 2015; Frost et al., 2010; Jackson et al., 2018; Mann et al., 2009; Ricolleau et al., 2011; Siebert et al., 2012; Takafuji & Hirose, 2005; Tsuno et al., 2013) and recently Mg (Badro et al., 2016, 2018; Du et al., 2017). The incorporation of both Si and O into the core during core-mantle differentiation provides a mechanism to account for the core's density deficit. The thermodynamic properties of the molten Fe–Si–O ternary are therefore essential to understand the thermal and chemical evolution of the core. The conditions (pressure, temperature, and composition) of metal-silicate equilibration during core formation set the composition of the bulk core by the end of accretion, and this is considered frozen from then onward. This last hypothesis is supported by the fact that the mantle cannot be in chemical equilibrium with the core (Jacobson et al., 2014; Stevenson, 1981; on the basis of highly siderophile element mantle abundances) and that the core and mantle have remained essentially isolated chemically after the end of core formation. Recently, Hirose et al. (2017) proposed a scenario that relaxes that hypothesis, where dissolved Si and O in the core would crystallize during secular cooling and float out due to its negative buoyancy, hence changing core composition over time.

One caveat of that study is that the proposed SiO_2 crystallization model and temperature were calculated from a thermodynamic model based on high-pressure metal-silicate equilibrium experiments. But those same experiments (e.g., Badro et al., 2016, 2018; Blanchard et al., 2017; Bouhifd & Jephcoat, 2011; Chidester et al., 2017; Du et al., 2017; Fischer et al., 2015; Huang & Badro, 2018; Jackson et al., 2018; Ricolleau et al., 2011; Siebert et al., 2012, 2013; Tsuno et al., 2013) have not observed any SiO_2 exsolution and even support that the present-day core could be undersaturated in Si and O (Brodholt & Badro, 2017). Since this discrepancy has never been addressed from a theoretical standpoint, we performed ab initio molecular dynamics (AIMD) simulations on liquid Fe–Si–O ternaries, Fe–O and Fe–Si binaries, and pure Fe at core-mantle boundary (CMB) pressure (136 GPa) and temperatures ranging from 3800 to 4800 K, covering the whole range of CMB temperatures from the Hadean eon to the present (Nimmo, 2015).

2. Methods

AIMD simulations were performed using Vienna Ab initio Simulation Package (Kresse & Hafner, 1993) with the projector augmented wave (PAW) method (Blöchl, 1994; Kresse & Joubert, 1999). The PAW potentials for iron, silicon, and oxygen have valence configurations of $3p^64s^13d^7$, $3s^23p^2$, and $2s^22p^4$ and core radii of 1.16, 1.31, and 0.82 Å, respectively. Perdew-Wang (Wang & Perdew, 1991) type generalized gradient approximation (GGA) was used for exchange-correlation functional. The energy cutoff for the plane wave expansion was 500 eV, with Γ point to sample the Brillouin zone. Simulations at high cutoff energy (900 eV) and a denser (2*2*2) k-point grid were run on various snapshots from each molecular dynamics (MD) run, in order to estimate the Pulay stress, which was found to be less than 0.6 GPa. Temperature was controlled using a Nosé-Poincaré thermostat. Single-particle orbitals were occupied according to the Fermi-Dirac distribution with an electronic temperature equal to the macroscopic temperature.

Two types of simulations were performed: single-phase liquid simulations and two-phase solid-liquid simulations. In the single-phase simulations, a box containing 108 Fe atoms was first heated up to 6000 K at 136 GPa for 20 ps to obtain a well-mixed liquid structure then cooled to four different temperatures relevant to the CMB (3800, 4000, 4300, and 4800 K). Then, some Fe atoms were replaced by Si and O atoms to obtain six different compositions ($Fe_{99}Si_9$, $Fe_{86}Si_{22}$, $Fe_{99}O_9$, $Fe_{86}O_{22}$, $Fe_{90}Si_9O_9$, and $Fe_{86}Si_{11}O_{11}$). In the two-phase simulations, a box containing 100 Fe atoms in the liquid state was equilibrated with a box containing 32 SiO_2 units in the solid seifertite structure at three different temperatures (3800, 4100, and 4300 K). The systems were run at constant NVT (canonical ensemble) for 20–63 ps with a time step of 1 fs to attain full equilibration and adequate statistics on thermodynamic functions. The first 1 ps were discarded and intensive variables such as P and T were calculated from the time average. The statistical uncertainties were evaluated using the blocking method (Flyvbjerg & Petersen, 1989) and give uncertainties in pressure between 0.1 and 0.2 GPa. A typical GGA underestimate of 10 GPa under CMB conditions was corrected following previous studies (Alfè et al., 2002; Badro et al., 2014).

3. Results and Discussion

3.1. Liquid Structure

In all our single-phase ternary ($Fe_{90}Si_9O_9$ and $Fe_{86}Si_{11}O_{11}$) simulations, liquid structure is confirmed by the partial radial distribution functions (RDFs). They are defined as the probability of finding an atom of species β in a shell dr at the distant r of the species α, given by

$$g_{\alpha\beta}(r) = \frac{dN_\beta(r)}{4\pi r^2 n_\beta dr},$$

(1)

where n_β is the number density of species β and $dN_\beta(r)$ the number of β atoms in the spherical shell $(r, r + dr)$ around a reference atom of species α (there are six possibilities in a three-component system, for example, $g_{FeFe}(r)$, $g_{SiSi}(r)$, $g_{OO}(r)$, $g_{FeSi}(r)$, $g_{FeO}(r)$, and $g_{SiO}(r)$). We average the RDFs over different sizes of time windows along the whole simulation and find no fundamental differences based on the choice of windows, which confirms that the system is well equilibrated. Figure 1a shows the partial RDFs of a typical liquid structure for the ternary $Fe_{86}Si_{11}O_{11}$ at 136 GPa and 3800 K. As can be seen from the position of the first peak of $g_{OO}(r)$, the distance to the nearest neighboring oxygens (~2.3 Å) is significantly larger than the Fe–O (~1.8 Å) or Si–O (~1.7 Å) distances. This indicates that oxygen has two effective radii in liquid iron alloy, a small
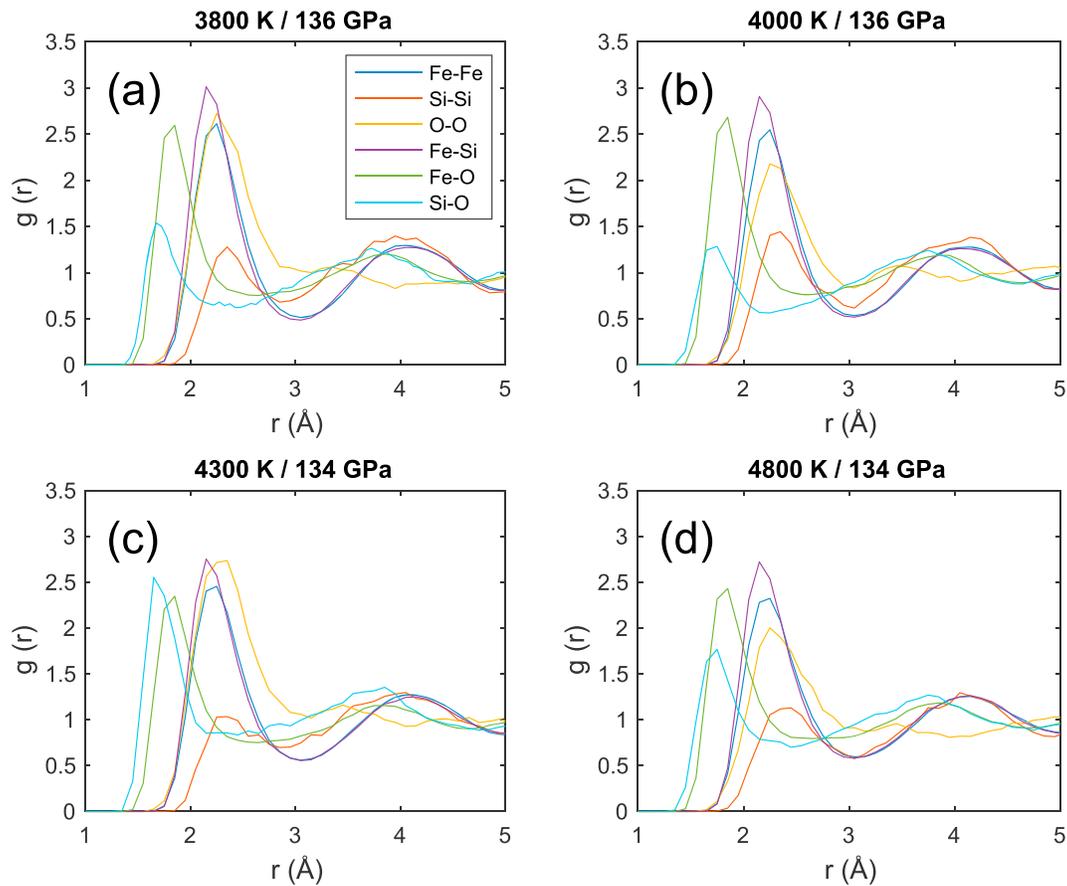
Figure 1. Partial radial distribution functions $g(r)$ for the $Fe_{86}Si_{11}O_{11}$ mixture at (a) 3800 K, (b) 4000 K, (c) 4300 K, and (d) 4800 K at core-mantle boundary pressure.

one when bonding with iron or silicon and a large one when interacting with itself, which is in excellent agreement with previous simulations on Fe–O and Fe–Si–O mixtures (Alfè et al., 1999; Pozzo et al., 2013). The bond lengths of Fe–Fe, Si–Si, and Fe–Si are similar between 2.2 to 2.3 Å, showing that iron and silicon atoms have similar and single effective radii when interacting with each other or themselves (Brodholt & Badro, 2017). Comparing partial RDFs at different temperatures spanning 1000 K at CMB pressure (between 3800 and 4800 K) shows that no resolvable changes of RDF patterns can be observed. The first peak in $g_{SiO}(r)$ is effectively the weakest, and on the same order as the second neighbor peak, showing no Si–O bond clustering, which would indicate the formation of SiO_2 units. This is further strengthened by an analysis of the coordination numbers of the ions in the melt.

The coordination number $C_{\alpha\beta}$ (the average number of atoms β around an atom α) is calculated by integrating the first peak of the RDFs and is plotted in Figure S1 in the supporting information:

$$C_{\alpha\beta} = 4\pi\, n_\beta \int_0^{r_{\min}} r^2\, g_{\alpha\beta}(r)dr, \tag{2}$$

where $r_{\min}$ is the position of the first minimum in $g_{\alpha\beta}$. The total number of neighbors (Fe + Si + O) surrounding each iron atom is constant (~13.5), which is consistent with previously observed numbers (between 13 and 14) in liquid Fe under core conditions (Umemoto & Hirose, 2015; Vočadlo et al., 1997). The number of oxygen neighbors of each silicon atom is systematically lower than 1, from 3800 to 4800 K, indicating nonstoichiometric (SiO_2) bonding and ruling out the formation of SiO_2 units.

It is noteworthy that the shortest distance exists between silicon and oxygen, indicating a shorter and probably stronger Si–O bond compared to all the other bonds. This should therefore make it easier to precipitate silicon and oxygen as SiO_2 from liquid iron or equivalently to block the dilution of Si and O in the

metal. In order to test this hypothesis, our Fe–Si–O ternary compositions were intentionally designed starting with silicon and oxygen atoms gathered at the same part of the simulation box, effectively simulating a two-phase system with pure iron on one end and an Si–O liquid on the other end. At all temperatures down to 3800 K, silicon and oxygen quickly mixed with iron as seen from the snapshots of MD trajectories (Figure S2 and Movie S1), yielding well-mixed liquid Fe–Si–O mixture, which opposes the tendency of the liquid to undergo phase separation.

3.2. Dynamics and Diffusion

Another line of argumentation stems from the analysis of atomic mean square displacements (MSDs) in the liquid, plotted in Figure 2. The MSD is given by an Einstein relation:

$$MSD(t) = \frac{1}{N_p}\sum_{i=1}^{N_p}\left\langle|\boldsymbol{r}_i(t+t_0)-\boldsymbol{r}_i(t_0)|^2\right\rangle, \tag{3}$$

where N_p is the number of particles, $\boldsymbol{r}_i$ is the position of the particle i at time t, and $<\cdot>$ represents ensemble average, which can be evaluated by averaging over different time origins t_0 along the simulation. During the first 20 fs, the atoms are moving freely before colliding with each other, as plotted in Figure 2 where the initial MSD increases as the square of time. After 200 fs the MSD establishes a linear behavior with time, which is typical of liquid structure (e.g., Pozzo et al., 2013; Umemoto & Hirose, 2015). The self-diffusion coefficient (D) is obtained from the linear part of MSD by

$$D = \frac{1}{6}\lim_{t\to\infty}\frac{\mathrm{d}MSD(t)}{\mathrm{d}t}. \tag{4}$$

As expected, the diffusion coefficient increases with temperature (Figure 2). At 136 GPa and 3800 K, we find $D_{Fe} = 0.4\cdot10^{-8}$ m^2/s, $D_{Si} = 0.3\cdot10^{-8}$ m^2/s, and $D_O = 1.0\cdot10^{-8}$ m^2/s: Fe and Si have very similar diffusion coefficients, whereas D_O is about 3 times faster. These data agree with those obtained from liquid iron ($D_{Fe} = 0.4–0.5\cdot10^{-8}$ m^2/s; Posner, Rubie, et al., 2017; Vočadlo et al., 1997), Fe–O ($D_{Fe} = 0.8\cdot10^{-8}$ m^2/s and $D_O = 10^{-8}$ m^2/s; Alfè et al., 1999; Posner, Steinle-Neumann, et al., 2017), Fe–Si–O ($D_{Fe} = D_{Si} = 0.4–0.5\cdot10^{-8}$ m^2/s and $D_O = \sim1.3\cdot10^{-8}$ m^2/s; Pozzo et al., 2013) under core conditions. This excellent agreement further confirms that the Fe$_{86}$Si$_{11}$O$_{11}$ mixture remains a single well-mixed liquid under all conditions (Figure S3).

3.3. Mixing Properties and Ideality

The properties of multicomponent iron alloys have often been calculated from those of the binaries based on ideal mixing of volumes (Badro et al., 2014; Brodholt & Badro, 2017; Huang et al., 2013). While this serves a tremendous purpose of using available data to explore core compositions at relevant P-T in complex systems, it has yet to be proven valid. For the sake of seismic properties of liquid planetary cores, the relevant material properties are density (i.e., volume) and bulk sound velocity (i.e., density and isentropic bulk modulus). Ideal mixing assumes that there is no excess volume upon mixing, that is, linear addition of end member volumes instead, described by

$$V_{mix} = V_{Fe} + \frac{\partial V}{\partial x_O}x_O + \frac{\partial V}{\partial x_{Si}}x_{Si}, \tag{5}$$

where V_{mix} is the volume of the ideal mixture; V_{Fe}, the volume of pure iron; and $\frac{\partial V}{\partial x_O}$ or $\frac{\partial V}{\partial x_{Si}}$, the partial derivative of volume with respect to O (x_O) and Si (x_{Si}) concentration, respectively.

Figure 3a shows the volume (and Figure 3b, density) as a function of composition, for Fe–O and Fe–Si binaries, as well as Fe–Si–O ternaries. All calculations are performed at CMB conditions of 4300 K and 136 GPa (see details in supporting information). The binaries are calculated for two O and Si concentrations and show that increasing light element concentration in iron always decreases density, as observed in previous simulations (Badro et al., 2014; Brodholt & Badro, 2017; Umemoto & Hirose, 2015). The perfect linear relationship between volume (or density) and concentration (i.e., no curvature as a function of concentration in Figures 3a and 3b) for the Fe–O and Fe–Si binaries demonstrates that iron and silicon or oxygen form perfectly ideal volume mixtures. As for ternaries, the volumes (and densities) were calculated in two ways:

AGU
100
ADVANCING EARTH
AND SPACE SCIENCE

Geophysical Research Letters

10.1029/2019GL082722
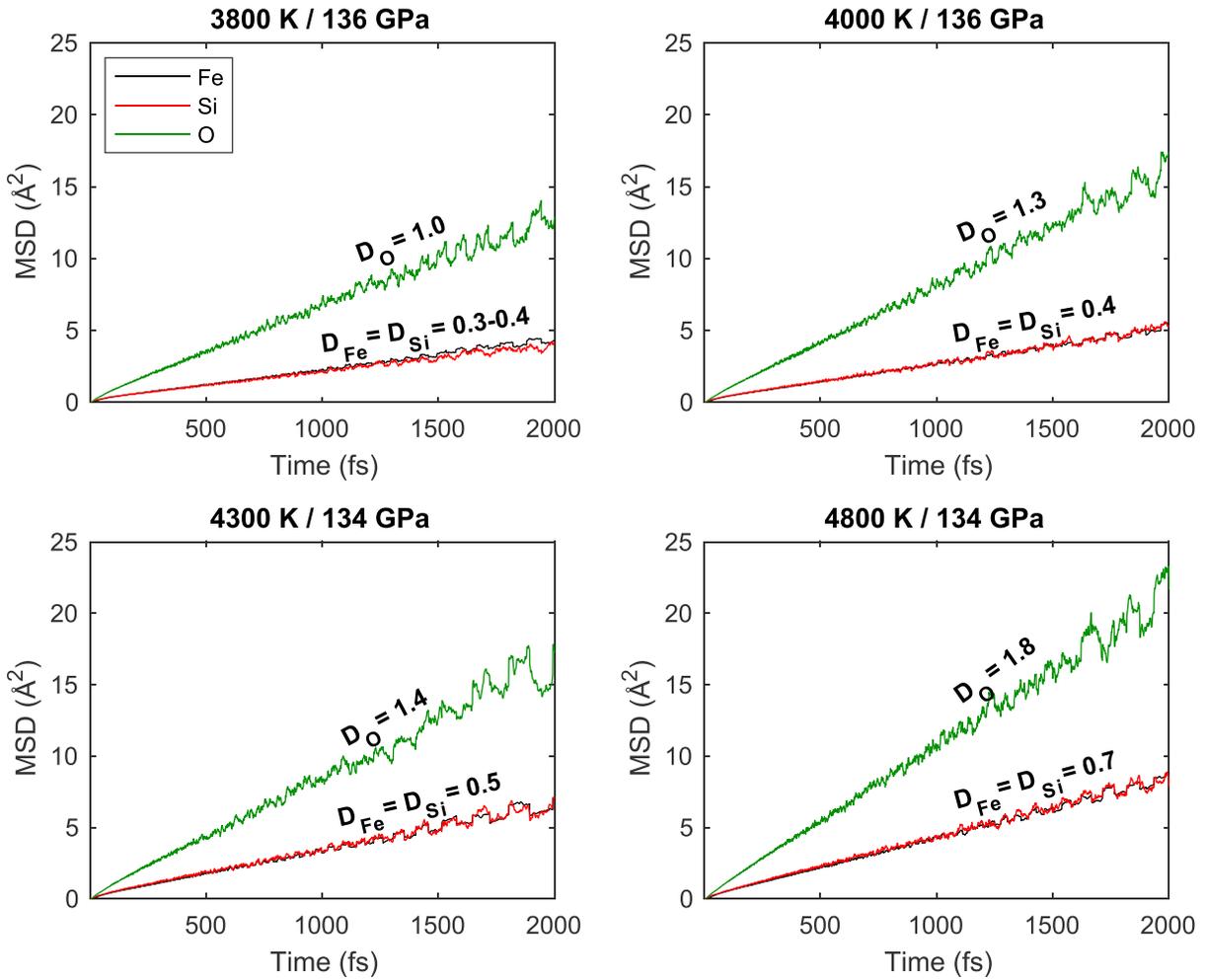
Figure 2. Mean square displacement of Fe, Si, and O as a function of time for the $Fe_{86}Si_{11}O_{11}$ mixture from 3800 to 4800 K at core-mantle boundary pressure. The linear behavior of mean square displacements is typical of a liquid structure. Self-diffusion coefficients of Fe, Si, and O atoms are labeled above the corresponding curves.
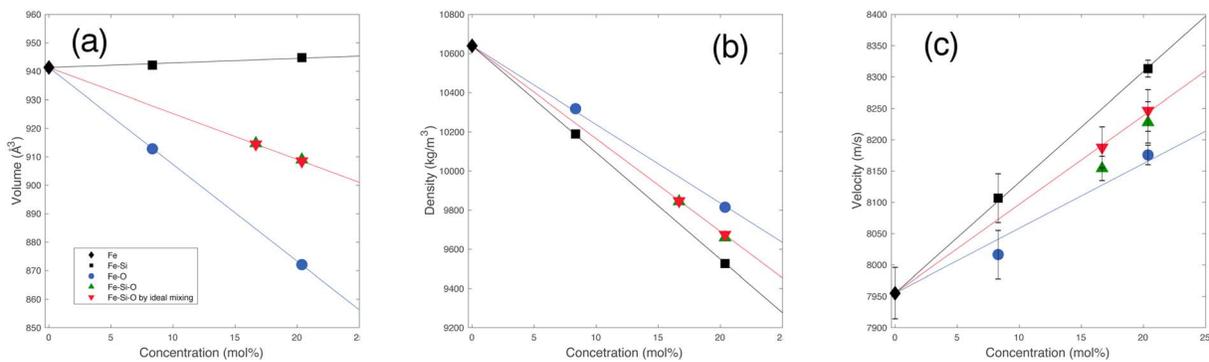
Figure 3. Volume (of 108 atoms), density, and bulk sound velocity of liquid Fe–X mixtures as a function of Si and (or) O concentration at core-mantle boundary conditions (4300 K and 136 GPa). Error bars are shown when larger than the symbols. Linear behaviors (black line for Si, blue line for O, and red line for Si + O) of volume, density, and velocity with increasing light element concentrations demonstrate the ideality of mixing Fe, Si, and O. The identical volumes, densities, and velocities of the calculated (green upward-pointing triangles) $Fe_{90}Si_9O_9$ and $Fe_{86}Si_{11}O_{11}$ ternaries and the ideally mixed ternaries (red downward-pointing triangles) show the Fe–Si–O mixtures can be produced by mixing Fe–Si and Fe–O binaries.

one was by actual MD simulations on the previously described ternary compositions ($Fe_{90}Si_9O_9$ and $Fe_{86}Si_{11}O_{11}$) and one by mixing the binaries according to equation (5). It is striking that both calculations produce identical results, proving that the generally assumed hypothesis of ideal mixing of volumes (Badro et al., 2014; Brodholt & Badro, 2017; Huang et al., 2013) of binaries is indeed valid at CMB conditions. In other words, Fe–Si–O ternary mixtures can be formed by ideal mixing of Fe–O and Fe–Si binary volumes under CMB conditions. The conclusion also holds for velocities, which are derivative properties (bulk modulus is the derivative of pressure with respect to volume), plotted in Figure 3c; the bulk sound velocities of the ternaries $Fe_{90}Si_9O_9$ and $Fe_{86}Si_{11}O_{11}$ equal those obtained by ideally mixing the volumes of binaries, within uncertainties.

3.4. SiO_2 Exsolution and Immiscibility in the Fe–Si–O Liquid

In solution crystallization, clusters with a short-range order usually form before the precipitation/crystallization of nuclei (Erdemir et al., 2009; Schenk et al., 2002). This comes with the change of bonding environments for the elements that are going to precipitate. As our structural analysis (partial RDF and coordination number) shows no change in the Si–O environment, the ternary liquids should be far from the conditions for SiO_2 crystallization. Another evidence comes from diffusion properties in liquid iron alloy. Our calculated diffusion rates of Fe, Si, and O agree well with previous calculations and experiments on liquid Fe, Fe–O, Fe–Si, or Fe–Si–O under core conditions (Alfè et al., 1999; Posner, Rubie, et al., 2017; Posner, Steinle-Neumann, et al., 2017; Pozzo et al., 2013; Vočadlo et al., 1997). In particular, the well-equilibrated liquid $Fe_{0.79}Si_{0.08}O_{0.13}$ ternary at 4000 K and 136 GPa from Pozzo et al. (2013) not only provides almost identical diffusion coefficients of Fe, Si, and O as in our calculations but also is at odds with the proposed SiO_2 exsolution isotherms (Hirose et al., 2017) by having higher concentrations of Si and O than what the precipitation model allows for (Figure S3). The discrepancy between the SiO_2 exsolution model and ab initio calculations could possibly be due to the thermodynamic model used by Hirose et al. (2017) to predict SiO_2 saturation temperature. While their low-pressure model fits well with existing metal-silicate partitioning data, their high-pressure model that suggests a lower saturation value is obtained by extrapolation and needs to be evaluated in the light of recent higher P-T metal-silicate partitioning data (Badro et al., 2018).

Our simulations in the Fe–Si–O ternary showed no phase separation, which is a necessary but not sufficient condition to address the possibility of SiO_2 exsolution. This is in contrast with a recent experimental and first-principle calculation study (Arveson et al., 2019) where SiO_2 exsolution was not observed but where the presence of Fe–Si and Fe–Si–O immiscible liquids was proposed. Here no immiscibility between Fe–Si and Fe–Si–O liquids was observed in the liquid state as described above, but instead liquid Fe–Si–O is well mixed at temperatures down to 3800 K and 136 GPa. As in Arveson et al. (2019), we analyzed the trajectories of Si and O in our $Fe_{86}Si_{11}O_{11}$ ternary at 3800 K, which is close to one of their simulated compositions. Si and O were initially clustered (as described previously), and the trajectories are plotted after 10, 20, and 29 ps in Figure 4, showing full mixing in the longest simulation runs. These are significantly longer than the simulations in Arveson et al. (2019), whose trajectories showing immiscibility were run for 6.6 to 14.8 ps. Such short simulation times do not allow to fully mix the system, as confirmed by our trajectories after 10 and 20 ps. In fact, both our results and theirs are consistent at short times (see the 10 ps run in Figure 4), and our interpretation is that although their simulations should produce the proper behavior, they were not run for long enough times to see full mixing.

Two computational methods allow to be more conclusive on the SiO_2 exsolution as well as the phase separation issue: Gibbs free-energy calculations of all the phases or long two-phase simulations (reversals) that circumvent the ergodicity requirement of the direct exsolution/phase separation case. The latter solution was favored here, and we reversed the experiment by investigating a two-phase simulation in a larger box containing solid SiO_2 (96 atoms) in the seifertite structure (e.g., Grocholski et al., 2013; Zhang et al., 2016) in contact with liquid Fe (100 atoms) at various temperatures (3800, 4100, and 4300 K). Above 4100 K, the SiO_2 and Fe phases mix in a short time (less than 10 ps); see Movies S2 and S3. At lower temperature, the process is much slower and becomes hard to see at 3800 K (Movie S4) even for longer simulation times (63 ps). Kinetics are also at work; no observed dissolution does not mean that the system does not dissolve (false negative), but observing dissolution necessarily means the system dissolves (true positive). While we cannot place a lower bound on the temperature at which SiO_2 exsolves, we clearly can say that it should not exsolve at 4100 K or above. The same holds for immiscibility in the liquid state.
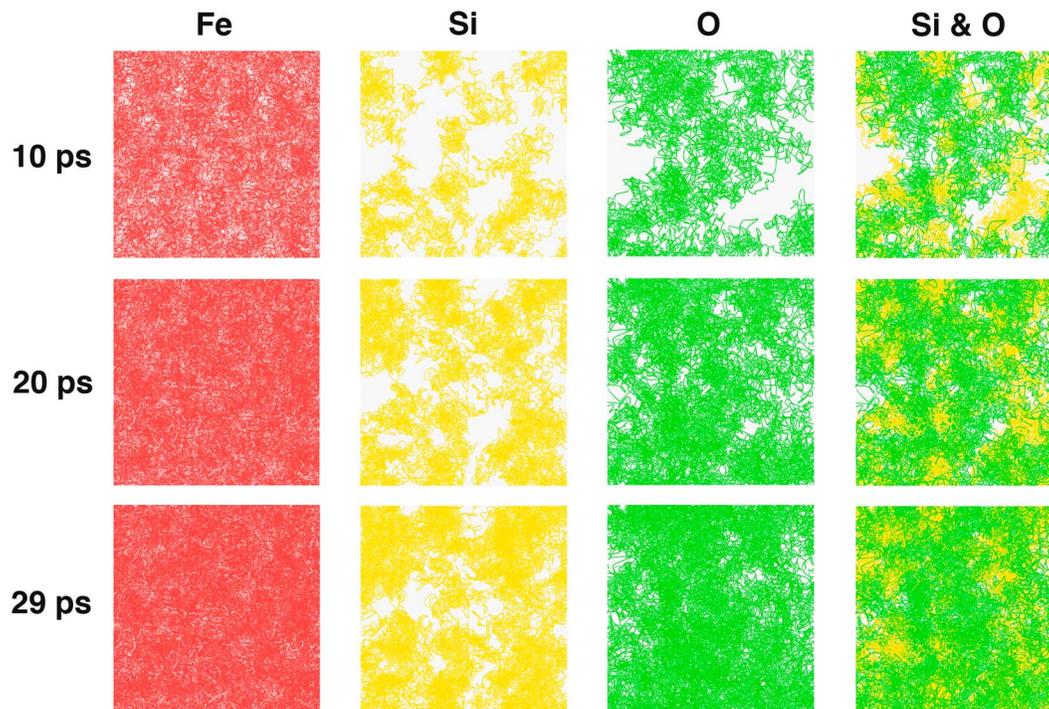
Figure 4. Fe, Si, and O atoms trajectories for three durations of the molecular dynamics simulations (10, 20, and 29 ps) for the $Fe_{86}Si_{11}O_{11}$ mixture at 3800 K and 136 GPa. The system starts (see main text) with Si and O clustered in one part of the box and is allowed to evolve; 3800 K is the lowest temperature studied here and should be the most favorable for observing exsolution (Hirose et al., 2017) or immiscibility (Arveson et al., 2019). However, the system evolves toward full mixing in about 30 ps. The initial topology (spaces devoid of oxygen or silicon) is still observed at 10 ps but slowly vanishes with longer simulation times to disappear at ~30 ps; no immiscibility observed between Fe–Si and Fe–Si–O liquids. Shorter (10 ps) simulations give the impression of immiscibility, and those durations are comparable to the ones (6 to 14 ps) used in Arveson et al. (2019). The two sets of simulations are therefore consistent, but the observed immiscibility seems an artifact due to the nonergodicity of the system at short times.

4. Conclusions

Using AIMD simulations, we investigated Fe–Si–O ternaries from 3800 to 4800 K at CMB pressure (136 GPa), along with Fe–O and Fe–Si binaries in the same conditions. Partial RDFs and coordination numbers agree well with previously reported liquid structures and show no sign of SiO_2 clustering. The analysis of the MSD of the atoms shows a typical liquid structure. Ternaries formed by ideal volume mixing of Fe–Si and Fe–O binaries have identical density and bulk sound velocity as those obtained in the calculated ternary, implying that equations of state of binary liquids (Fe–Si and Fe–O) can be used to obtain reliable equations of state of Fe–Si–O ternary alloys at core conditions. Finally, two-phase simulations starting with solid SiO_2 + liquid Fe and liquid Si–O + liquid Fe show rapid and full mixing of Fe, Si, and O, supporting a well-mixed system and suggesting no phase separation or immiscibility. This implies no sign of SiO_2 exsolution from the core nor any sign of Fe–Si–O two-liquid immiscibility down to at least 3800 K, which is a lower bound on the present-day temperature at the CMB.

References

Alfè, D., Price, G. D., & Gillan, M. J. (2002). Iron under Earth's core conditions: Liquid-state thermodynamics and high-pressure melting curve from *ab initio* calculations. *Physical Review B: Condensed Matter and Materials Physics*, *65*(16), 165118. https://doi.org/10.1103/PhysRevB.65.165118

Alfè, D., Price, G. D., & Gillan, M. J. (1999). Oxygen in the Earth's core: A first-principles study. *Physics of the Earth and Planetary Interiors*, *110*(3–4), 191–210. https://doi.org/10.1016/S0031-9201(98)00134-4

Arveson, S. M., Deng, J., Karki, B. B., & Lee, K. K. M. (2019). Evidence for Fe-Si-O liquid immiscibility at deep Earth pressures. *Proceedings of the National Academy of Sciences of the United States of America*, *116*(21), 10,238–10,243. https://doi.org/10.1073/pnas.1821712116

Asahara, Y., Frost, D. J., & Rubie, D. C. (2007). Partitioning of FeO between magnesiowüstite and liquid iron at high pressures and temperatures: Implications for the composition of the Earth's outer core. *Earth and Planetary Science Letters*, *257*(3-4), 435–449. https://doi.org/10.1016/j.epsl.2007.03.006

Badro, J., Aubert, J., Hirose, K., Nomura, R., Blanchard, I., Borensztajn, S., & Siebert, J. (2018). Magnesium partitioning between Earth's mantle and core and its potential to drive an early exsolution geodynamo. *Geophysical Research Letters*, *45*, 13,240–13,248. https://doi.org/10.1029/2018GL080405

Badro, J., Cote, A. S., & Brodholt, J. P. (2014). A seismologically consistent compositional model of Earth's core. *Proceedings of the National Academy of Sciences of the United States of America*, *111*(21), 7542–7545. https://doi.org/10.1073/pnas.1316708111

Badro, J., Siebert, J., & Nimmo, F. (2016). An early geodynamo driven by exsolution of mantle components from Earth's core. *Nature*, 1–3. https://doi.org/10.1017/CBO9781107415324.004

Blanchard, I., Siebert, J., Borensztajn, S., & Badro, J. (2017). The solubility of heat-producing elements in Earth's core. *Geochemical Perspectives Letters*, 1–5. https://doi.org/10.7185/geochemlet.1737

Blöchl, P. E. (1994). Projector augmented-wave method. *Physical Review B: Condensed Matter and Materials Physics*, *50*(24), 17,953–17,979. https://doi.org/10.1103/PhysRevB.50.17953

Bouhifd, M. A., & Jephcoat, A. P. (2011). Convergence of Ni and Co metal–silicate partition coefficients in the deep magma-ocean and coupled silicon–oxygen solubility in iron melts at high pressures. *Earth and Planetary Science Letters*, *307*(3–4), 341–348. https://doi.org/10.1016/j.epsl.2011.05.006

Brodholt, J., & Badro, J. (2017). Composition of the low seismic velocity E′ layer at the top of Earth's core. *Geophysical Research Letters*, *44*, 8303–8310. https://doi.org/10.1002/2017GL074261

Chabot, N. L., & Agee, C. B. (2003). Core formation in the Earth and Moon: New experimental constraints from V, Cr, and Mn. *Geochimica et Cosmochimica Acta*, *67*(11), 2077–2091. https://doi.org/10.1016/S0016-7037(02)01272-3

Chidester, B. A., Rahman, Z., Righter, K., & Campbell, A. J. (2017). Metal-silicate partitioning of U: Implications for the heat budget of the core and evidence for reduced U in the mantle. *Geochimica et Cosmochimica Acta*, *199*, 1–12. https://doi.org/10.1016/j.gca.2016.11.035

Du, Z., Jackson, C., Bennett, N., Driscoll, P., Deng, J., Lee, K. K. M., et al. (2017). Insufficient energy from MgO exsolution to power early geodynamo. *Geophysical Research Letters*, *44*, 11,376–11,381. https://doi.org/10.1002/2017GL075283

Erdemir, D., Lee, A. Y., & Myerson, A. S. (2009). Nucleation of crystals from solution: Classical and two-step models. *Accounts of Chemical Research*, *42*(5), 621–629. https://doi.org/10.1021/ar800217x

Fischer, R. A., Nakajima, Y., Campbell, A. J., Frost, D. J., Harries, D., Langenhorst, F., et al. (2015). High pressure metal-silicate partitioning of Ni, Co, V, Cr, Si, and O. *Geochimica et Cosmochimica Acta*, *167*, 177–194. https://doi.org/10.1016/j.gca.2015.06.026

Flyvbjerg, H., & Petersen, H. G. (1989). Error estimates on averages of correlated data. *The Journal of Chemical Physics*, *91*(1), 461–466. https://doi.org/10.1063/1.457480

Frost, D. J., Asahara, Y., Rubie, D. C., Miyajima, N., Dubrovinsky, L. S., Holzapfel, C., et al. (2010). Partitioning of oxygen between the Earth's mantle and core. *Journal of Geophysical Research*, *115*, B02202. https://doi.org/10.1029/2009JB006302

Grocholski, B., Shim, S., & Prakapenka, V. B. (2013). Stability, metastability, and elastic properties of a dense silica polymorph, seifertite. *Journal of Geophysical Research: Solid Earth*, *118*, 4745–4757. https://doi.org/10.1002/jgrb.50360

Hirose, K., Morard, G., Sinmyo, R., Umemoto, K., Hernlund, J., Helffrich, G., & Labrosse, S. (2017). Crystallization of silicon dioxide and compositional evolution of the Earth's core. *Nature*, *543*(7643), 99–102. https://doi.org/10.1038/nature21367

Huang, D., & Badro, J. (2018). Fe-Ni ideality during core formation on Earth. *American Mineralogist*, *103*(10), 1707–1710. https://doi.org/10.2138/am-2018-6651

Huang, H., Wu, S., Hu, X., Wang, Q., Wang, X., & Fei, Y. (2013). Shock compression of Fe-FeS mixture up to 204 GPa. *Geophysical Research Letters*, *40*, 687–691. https://doi.org/10.1002/grl.50180

Jackson, C. R. M., Bennett, N. R., Du, Z., Cottrell, E., & Fei, Y. (2018). Early episodes of high-pressure core formation preserved in plume mantle. *Nature*, *553*(7689), 491–495. https://doi.org/10.1038/nature25446

Jacobson, S. A., Morbidelli, A., Raymond, S. N., O'Brien, D. P., Walsh, K. J., & Rubie, D. C. (2014). Highly siderophile elements in Earth's mantle as a clock for the Moon-forming impact. *Nature*, *508*(7494), 84–87. https://doi.org/10.1038/nature13172

Kresse, G., & Hafner, J. (1993). Ab initio molecular dynamics for liquid metals. *Physical Review B: Condensed Matter and Materials Physics*, *47*(1), 558–561. https://doi.org/10.1103/PhysRevB.47.558

Kresse, G., & Joubert, D. (1999). From ultrasoft pseudopotentials to the projector augmented-wave method. *Physical Review B: Condensed Matter and Materials Physics*, *59*(3), 1758–1775. https://doi.org/10.1103/PhysRevB.59.1758

Mann, U., Frost, D. J., & Rubie, D. C. (2009). Evidence for high-pressure core-mantle differentiation from the metal-silicate partitioning of lithophile and weakly-siderophile elements. *Geochimica et Cosmochimica Acta*, *73*(24), 7360–7386. https://doi.org/10.1016/j.gca.2009.08.006

Nimmo, F. (2015). Thermal and compositional evolution of the core. In *Treatise on Geophysics* (Vol. 9, pp. 201–219). New York: Elsevier B. V. https://doi.org/10.1016/B978-044452748-6.00147-4

Posner, E. S., Rubie, D. C., Frost, D. J., Vlček, V., & Steinle-Neumann, G. (2017). High P–T experiments and first principles calculations of the diffusion of Si and Cr in liquid iron. *Geochimica et Cosmochimica Acta*, *203*, 323–342. https://doi.org/10.1016/j.gca.2017.01.024

Posner, E. S., Steinle-Neumann, G., Vlček, V., & Rubie, D. C. (2017). Structural changes and anomalous self-diffusion of oxygen in liquid iron at high pressure. *Geophysical Research Letters*, *44*, 3526–3534. https://doi.org/10.1002/2017GL072926

Pozzo, M., Davies, C., Gubbins, D., & Alfè, D. (2013). Transport properties for liquid silicon-oxygen-iron mixtures at Earth's core conditions. *Physical Review B: Condensed Matter and Materials Physics*, *87*(1), 014110. https://doi.org/10.1103/PhysRevB.87.014110

Ricolleau, A., Fei, Y., Corgne, A., Siebert, J., & Badro, J. (2011). Oxygen and silicon contents of Earth's core from high pressure metal-silicate partitioning experiments. *Earth and Planetary Science Letters*, *310*(3–4), 409–421. https://doi.org/10.1016/j.epsl.2011.08.004

Ringwood, A. E. (1959). On the chemical evolution and densities of the planets. *Geochemica et Cosmochimica Acta*, *15*(4), 257–283. https://doi.org/10.1016/0016-7037(59)90062-6

Schenk, T., Simonet, V., Bellissent, R., & Herlach, D. M. (2002). Icosahedral short-range order in deeply undercooled metallic melts. *Physical Review Letters*, *89*(7), 1–4. https://doi.org/10.1103/PhysRevLett.89.075507

Siebert, J., Badro, J., Antonangeli, D., & Ryerson, F. J. (2012). Metal-silicate partitioning of Ni and Co in a deep magma ocean. *Earth and Planetary Science Letters*, *321–322*, 189–197. https://doi.org/10.1016/j.epsl.2012.01.013

Siebert, J., Badro, J., Antonangeli, D., & Ryerson, F. J. (2013). Terrestrial accretion under oxidizing conditions. *Science*, *339*(6124), 1194–1197. https://doi.org/10.1126/science.1227923

Stevenson, D. J. (1981). Models of the Earth's core. *Science*, *214*(4521), 611–619. https://doi.org/10.1126/science.214.4521.611

Takafuji, N., & Hirose, K. (2005). Solubilities of O and Si in liquid iron in equilibrium with (Mg, Fe) SiO_3 perovskite and the light elements in the core. *Geophysical Research Letters*, *32*, L06313. https://doi.org/10.1029/2005GL022773

Tsuno, K., Frost, D. J., & Rubie, D. C. (2013). Simultaneous partitioning of silicon and oxygen into the Earth's core during early Earth differentiation. *Geophysical Research Letters*, *40*, 66–71. https://doi.org/10.1029/2012GL054116

Umemoto, K., & Hirose, K. (2015). Liquid iron-hydrogen alloys at outer core conditions by first-principles calculations. *Geophysical Research Letters*, *42*, 7513–7520. https://doi.org/10.1002/2015GL065899

Vočadlo, L., de Wijs, G. A., Kresse, G., Gillan, M., & Price, G. D. (1997). First principles calculations on crystalline and liquid iron at Earth's core conditions. *Faraday Discussions*, *106*, 205–218. https://doi.org/10.1039/a701628j

Wang, Y., & Perdew, J. P. (1991). Correlation hole of the spin-polarized electron gas, with exact small-wave-vector and high-density scaling. *Physical Review B: Condensed Matter and Materials Physics*, *44*(24), 13,298–13,307. https://doi.org/10.1103/PhysRevB.44.13298

Zhang, L., Popov, D., Meng, Y., Wang, J., Ji, C., Li, B., & Mao, H. K. (2016). In-situ crystal structure determination of seifertite SiO_2 at 129 GPa: Studying a minor phase near Earth's core–mantle boundary. *American Mineralogist*, *101*(1), 231–234. https://doi.org/10.2138/am-2016-5525